System-Level Large-Signal Stability Analysis of Droop-Controlled DC Microgrids

Wenqiang Xie, *Student Member, IEEE*, Minxiao Han, *Senior Member, IEEE*, Wenyuan Cao, *Student Member, IEEE*, Josep M. Guerrero, *Fellow, IEEE*, and Juan C. Vasquez, *Senior Member, IEEE*

***Abstract*—In the literature, many studies on stability analysis of dc microgrids have been conducted. However, most of them mainly focus on small-signal stability. On the other hand, few works analyze large-signal stability, but the major part of these works is based on a single unit or a simple cascaded system as a case study. Different from those, this article aims to address the large-signal stability analysis of a dc microgrid from a system-level perspective. First, the equivalent model of a droop-controlled dc microgrid is developed. Subsequently, the Lyapunov-based large-signal stability analysis and the stability criterion are derived, and mixed potential theory is used to make comparisons to verify the effectiveness of the derived criterion. The equilibrium point stability for different operation stages was obtained by means of theoretical calculation. Furthermore, the instabilities principle as well as their physical interpretation is revealed. In this article, the bus voltage is used as the only index to assess the microgrid power balance. Hence, the power load limit can be obtained by taking into consideration the stability and voltage deviation constraints. Finally, simulation and experimental results from a four-converter dc microgrid system verify the feasibility of the proposed theoretical analysis.**

***Index Terms*—DC microgrids, droop control, large-signal stability, Lyapunov function.**

I. Introduction

As an effective way to seamlessly integrate and utilize distributed energy resources, dc microgrids have been extensively studied over the past ten years [1], [2]. These have been used in so many fields, including the power grid, industry, greenhouse, traffic, etc. Although dc microgrids have many benefits, many drawbacks still exist [3]–[5]. Stability is a vital issue that cannot be ignored as its weak inertia and damping [6]–[8]. Many studies about stability have been conducted through small-signal analysis (SSA) and large-signal analysis (LSA) [9]–[11].

SSA is based on linearizing the nonlinear system around an equilibrium point, and the linearized system is then studied by linear analysis tools such as eigenvalue, Nyquist, and Routh stability criterion. It has been widely applied in a single unit, including motors, inverters, and rectifiers, to improve parameter design in controllers [12], [13]. However, the main drawback of SSA is that its validity and effectiveness are limited to a tiny domain around an equilibrium point, without accurate indication of how large the tiny domain is. Moreover, the parameters designed by SSA are only accurate at a certain equilibrium point, but the equilibrium point is frequently changed as pulse power load operation and load switching.

Large power disturbances in dc microgrids are inevitable, such as loss of distributed sources, large load variations, and circuit faults [14], hence LSA is much necessary. LSA adopts nonlinear mathematical methods without linearization, whose complexity is determined by the order of the system, and the domain of which is much larger than that of SSA. Many studies have been done about LSA in recent years, but most of them focus on one unit or a cascaded system [15]–[18], thus not being appropriated for a system level. In this sense, Lin *et al.* [16] describe a dc microgrid as a cascaded system by a single source in connection with constant power load (CPL), and then optimizes parameter design based on double close-loop control, not suitable for the multisource parallel system. For instance, in [17] and [18], a control parameter determination method for grid-forming converters (GC) is proposed to stabilize the system under large-signal disturbances. The premise of this method is that the capacity of a single energy storage unit should be large enough since this approach can be only used for one voltage source [19].

Furthermore, in [16], LSA is used to estimate the domain of asymptotic stability of dc microgrids, but it mainly concentrates on the parameter design of the grid-connected inverter. On the other hand, usually, the capacity of the ac grid is large enough, hence it is commonly stable in grid-connected mode. Hence, more efforts should be put into the studies on islanded dc microgrids modeling. This article focuses on island dc microgrids stability modeling and analysis. With the scale-up of dc microgrids, more than one GC requires the parallel operation to provide enough capacity and redundancy. In this sense, droop

Manuscript received June 18, 2020; accepted August 10, 2020. Date of publication August 25, 2020; date of current version November 20, 2020. This work was supported in part by the National Key R&D Program of China under Grant 2018YFB0904700, in part by the Fundamental Research Funds for the Central Universities under Grant 2019QN119, and in part by VILLUM FONDEN under the VILLUM Investigator Grant 25920: Center for Research on Microgrids. Recommended for publication by Associate Editor F. W. Fuchs. *(Corresponding author: Wenqiang Xie.)*

Wenqiang Xie is with the School of Electrical and Electronic Engineering, North China Electric Power University, Beijing 102206, China, and also with the Department of Energy Technology, Aalborg University, 9220 Aalborg, Denmark (e-mail: bjxiewenqiang@163.com).

Minxiao Han and Wenyuan Cao are with the School of Electrical and Electronic Engineering, North China Electric Power University, Beijing 102206, China (e-mail: hanminxiao@263.net; bjcaowenyuan@163.com).

Josep M. Guerrero and Juan C. Vasquez are with the Department of Energy Technology, Aalborg University, 9220 Aalborg, Denmark (e-mail: joz@et.aau.dk; juq@et.aau.dk).

Color versions of one or more of the figures in this article are available online at https://ieeexplore.ieee.org.

Digital Object Identifier 10.1109/TPEL.2020.3019311

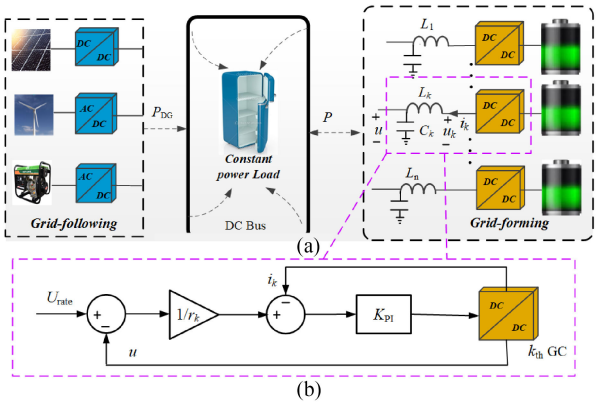

Fig. 1. Typical structure of dc microgrid and droop controller. (a) Typical structure. (b) Droop controller of $k_{\rm th}$ GC.

controller is widely employed in many studies [19], [20], which allows circulating current reduction among converters and can easily realize power-sharing and voltage regulation [21]–[23]. Thus, the single voltage-source model is no more appropriate for those multiple voltage-source converter systems. Most studies using single voltage-source models are engaged in optimizing proportional and integral (PI) controller parameters design [16]–[18]. However, a dc microgrid is a more complex system as shown in Fig. 1, in which lots of converters coexist. Each of them has its own proportional and integral parameters, which are usually set by the designer and unknown to the users. Thus, it is not practical to figure out one set of equivalent parameters when multi-GC parallel system is taken into consideration.

Many studies have illustrated that CPLs exhibit negative impedance characteristics, thus threatening the stable operations of dc microgrids. CPLs are commonly referred to those power electronic loads and motors with tight regulation, and so on. They present negative impedances to the dc bus within their control bandwidths and unfavorably interact with source converters [25], [26]. Considering CPLs have more negative influences than resistive load, the extremely worst situation that all loads are CPLs is studied in this article, making dc microgrids a nonlinear system.

Several methods can be used in LSA of nonlinear systems, including the Lyapunov direct method, Takagi–Sugeno fuzzy model method (TS), block diagonalized quadratic Lyapunov function (BDQLF), reverse trajectory tracking method, and mixed potential theory (MPT), but each of them has shortcomings. The Lyapunov direct method is the most widely used approach in estimating region of attraction [11], [20], [24], [27], although the derived stability criterion is commonly conservative. However, this drawback can be easily overcome in this article. The TS [28] and BDQLF [29] are derived from the Lyapunov direct method, which share the same problem of the conservative criterion. Additionally, the computational complexity of TS increases exponentially with the number of nonlinearities, making TS ill-suited for higher order systems. The reverse trajectory tracking method [30] is a graphical approach and cannot be derived in an analytic form. MPT is another

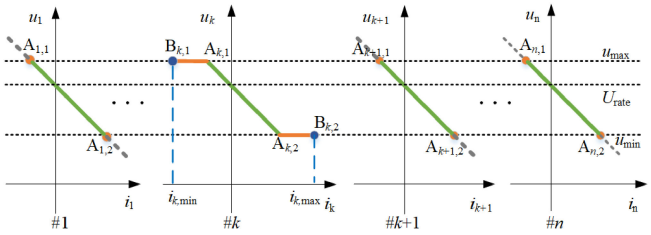

Fig. 2. Schematic diagram of control strategy of multi-GC parallel operation.

commonly utilized method in recent years [15], [16], [31], but its criterion is not as detailed as that derived by the Lyapunov direct method in this article, and it is hard to rigidly prove the necessity of the second condition in studies. Therefore, the Lyapunov direct method is adopted in this article, and conservatism-free is achieved mathematically. Besides, to illustrate the advantages of the Lyapunov direct method, MPT is employed in Section III to make comparisons.

The rest of the article is organized as follows. Section II develops the system model according to the operation strategy with droop control. Section III establishes the Lyapunov function to analyze large-signal stability, then the sufficiency and necessity criterion is derived. To tell the advantages of the Lyapunov direct method, MPT is employed to make comparisons. In Section IV, the stability of equilibrium points in different stages is discussed, and its physical interpretation is clearly explained. Furthermore, the limit of power load is proposed in Section V within the constraints of stability and voltage deviation. Simulation and experimental results are provided in Section VI to enhance the correctness of the theoretical analysis. Finally, Section VII concludes the article.

II. Large-Signal Model of DC Microgrids

A. Grid-Forming Converters Modeling

DC microgrids consist of distributed power sources, energy storage systems, and power loads, as shown in Fig. 1. With the scaling-up of dc microgrids, energy storage system requires more parallel-connected GCs to maintain power balance [32], [33]. Hence, droop control is widely employed. The voltage droop control can be implemented in a virtual-resistance way as follows:

$$u = U_{\rm rate} - ri \tag{1}$$

where $U_{\rm rate}$ is the rated voltage, u is the bus voltage, i is the load current, and r is the virtual resistance. According to (1), the external characteristic of droop control can be thought as the series connection of dc source and virtual resistance.

Assuming n GCs parallel operation in a dc microgrid and each adopting drool control strategy, the control curve can be shown in Fig. 2, where $n \in N = \{1, 2, \ldots, n\}$. Considering the requirement of insulation, devices operation, etc., the voltage deviation must be limited within a reasonable range. Besides, in order to avoid huge circulation caused by control deviations when parallel operation, only one GC (the master GC) can employ constant voltage strategy. Only if this GC fails to normal

operation, one of the other GCs can adopt the constant voltage strategy in accordance with certain priorities. Therefore, the operation process can be divided into two stages as shown in Fig. 2. In the first stage, voltage deviation does not reach any bound, so that all GCs adopt droop control. In the second stage, voltage deviation reaches upper or lower bound, thus one GC adopts constant voltage strategy and the others adopt constant current strategy. For convenient expression, here define two types of operating points A and B, where A is determined by voltage/current limitations and B by the converter capacity. Taking $k_{\rm th}$ GC as an example, [A_{k1}, $A_{k,2}$] is for droop control strategy, [B_{k1}, $A_{k,1}$] and [A_{k2}, $B_{k,2}$] are for constant voltage strategy.

1) Modeling for the First Stage: In the first stage, all GCs adopt droop control strategy. As shown in Fig. 1, the transient control model of $k_{\rm th}$ GC can be expressed as follows:

$$\frac{di_k}{dt} = \frac{1}{L_k}(U_{\rm rate} - u - r_k i_k) \tag{2}$$

where i_k is the output current of the $k_{\rm th}$ GC, L_k is the output side inductance in series with $k_{\rm th}$ GC, and r_k is the virtual resistance of the $k_{\rm th}$ GC.

Assuming $i_{\rm eq}$ as the output current of the entire energy storage system, it can be expressed as follows:

$$i_{\rm eq} = \sum_{k=1}^{n} i_k = (U_{\rm rate} - u)\sum_{k=1}^{n}\frac{1}{r_k}. \tag{3}$$

Hence, the equivalent virtual resistance can be expressed as follows:

$$r_{\rm eq} = 1\Big/\sum_{k=1}^{n}\frac{1}{r_k}. \tag{4}$$

Considering the condition in design [23]

$$\frac{r_1}{L_1} \approx \frac{r_2}{L_2} \approx \cdots \approx \frac{r_n}{L_n} \tag{5}$$

then, we can obtain the equivalent current dynamics by combining (3)–(5) as follows:

$$\frac{{\rm d}i_{\rm eq}}{{\rm d}t} = (U_{\rm rate} - u)\sum_{k=1}^{n}\frac{1}{L_k} - i_{\rm eq}\sum_{k=1}^{n}\frac{1}{L_k}\Big/\sum_{k=1}^{n}\frac{1}{r_k}. \tag{6}$$

Thus, the equivalent inductance $L_{\rm eq}$ can be approximately given by

$$L_{\rm eq} = 1\Big/\sum_{k=1}^{n}\frac{1}{L_k}. \tag{7}$$

Then, (6) can be reformulated as follows:

$$\frac{{\rm d}i_{\rm eq}}{{\rm d}t} = \frac{1}{L_{\rm eq}}\left(U_{\rm rate} - u - r_{\rm eq} i_{\rm eq}\right). \tag{8}$$

Therefore, a multi-GC parallel operation storage system adopting drool control can be also equivalent to the series connection of dc source, virtual resistance, and filter inductance, as shown in Fig. 3(a).

2) Modeling for the Second Stage: In the second stage, the $k_{\rm th}$ GC operates in constant voltage mode, where the output current is determined by power load. Besides, the other GCs will work in constant current mode because the bus voltage is constant. Hence, the equivalent circuit can be modeled as the series connection of dc source and filter inductance, and then parallel connected to a controlled current source, as shown in Fig. 3(b). The total output current and power of the other GCs can be separately represented by $i_{\rm oth}$ and $P_{\rm oth}$ as follows:

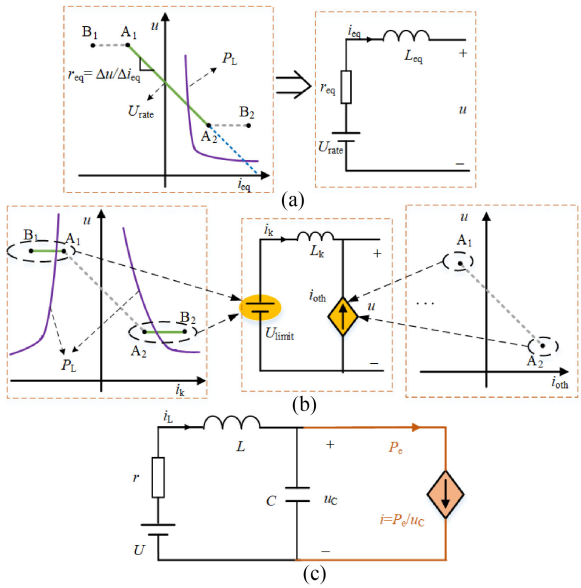

Fig. 3. Equivalent model of dc microgrid. (a) Equivalent circuit of the first stage. (b) Equivalent circuit of the second stage. (c) Normalized equivalent model of two stages.

$$P_{\rm oth} = i_{\rm oth}\cdot U_{\rm lim} = U_{\rm lim}\cdot\sum_{m\neq k} i_m \tag{9}$$

where $U_{\rm lim}$ is the limited value of voltage deviation. The other GCs operate as negative power load relative to the $k_{\rm th}$ GC.

B. Modeling for Equivalent Power Load

In order to maximize the utilization of renewable energy, distributed sources mostly operate in maximum power point tracking (MPPT) mode, which show like the reverse power loads relative to the energy storage system. It is positive when power flows to energy storage system from distributed energy and symbolled by $P_{\rm DG}$.

As aforesaid, the dc load in the dc microgrids exhibits constant power characteristics due to its power electronic converters with a tight feedback controller. From the perspective of the system, the dc load can be equivalent to the power load that varies with the usage behavior of electricity and expressed by $P_{\rm load}$.

Therefore, the distributed power source and the dc load can be equivalent to a bidirectional power load $P_{\rm L}$, expressed as

$$P_{\rm L} = P_{\rm load} - P_{\rm DG}. \tag{10}$$

C. Equivalent Model of DC Microgrids

Based on the above analysis, considering the capacitance parallel to the energy storage system, distributed energy, grid-connected unit, and dc bus, the normalized equivalent model of two stages of dc microgrids can be expressed as in Fig. 3(c), where U is the equivalent dc voltage source, r is the equivalent virtual resistance, L is the equivalent inductance, $P_{\rm e}$ is the equivalent constant power load, and C is the equivalent capacitance connected in parallel to the dc bus. Besides, $u_{\rm C}$ is the capacitance voltage, i.e., the bus voltage, $i_{\rm L}$ is the inductance current, $i = P/u_{\rm C}$ is the equivalent load current, and $i = i_{\rm L}$ is the steady-state.

It is easy to conclude that the means of variables in the first stage and second stage separately are as follows:

$$\text{first stage}\begin{cases} U = U_{\rm rate} \\ r = r_{\rm eq} \\ L = L_{\rm eq} \\ P_{\rm e} = P_{\rm L} \end{cases}, \text{second stage}\begin{cases} U = U_{\rm lim} \\ r \to 0 \\ L = L_{\rm k} \\ P_{\rm e} = P_{\rm L} - P_{\rm oth}. \end{cases} \tag{11}$$

III. Large-Signal Stability Criterion

The Lyapunov function is established in this section to analyze large-signal stability of dc microgrids, and MPT is employed to make comparisons with it. The results show that the Lyapunov direct method is more suitable for this article.

A. LSA Based on the Lyapunov Direct Method

Assuming $x_{\rm e} = [i_{\rm Le}, u_{\rm Ce}]^{\rm T}$ as the equilibrium point of the system, and $\Delta x = [\Delta i_{\rm L}, \Delta u_{\rm C}]^{\rm T}$ as variation, the mathematical model of dc microgrids can be derived as follows:

$$\begin{cases} \frac{d(\Delta i_{\rm L})}{dt} = \frac{1}{L}(-r\Delta i_{\rm L} - \Delta u_{\rm C}) \\ \frac{d(\Delta u_{\rm C})}{dt} = \frac{1}{C}(\Delta i_{\rm L} + \frac{P_{\rm e}}{u_{\rm Ce}^2}\Delta u_{\rm C}). \end{cases} \tag{12}$$

Its matrix form is

$$\Delta\dot{\boldsymbol{x}} = \boldsymbol{J}\Delta\boldsymbol{x} \tag{13}$$

where

$$\boldsymbol{J} = \begin{bmatrix} -r/L & -1/L \\ 1/C & P_{\rm e}/Cu_{\rm C}^2 \end{bmatrix}_{x_e}. \tag{14}$$

According to the Lyapunov direct method, for a given nonlinear system, if a Lyapunov function $\boldsymbol{V}(\boldsymbol{x})$ is found to be a positive definite matrix and meanwhile its derivative is a negative definite matrix, then the system is of small-signal stability at the equilibrium point. In addition, when $\|\boldsymbol{x}\|\to\infty$, $\boldsymbol{V}(\boldsymbol{x})\to\infty$ is further satisfied, the system is believed to be large-signal stable. For the system built as (12)–(14), that $\boldsymbol{x} = [i_{\rm L}, u_{\rm C}]^{\rm T}$ is selected as state variables, and then the equation of state can be expressed as follows:

$$\dot{\boldsymbol{x}} = \boldsymbol{\Phi}(\boldsymbol{x}) \tag{15}$$

and

$$\dot{\boldsymbol{\Phi}}(\boldsymbol{x}) = \frac{\partial\boldsymbol{\Phi}(\boldsymbol{x})}{\partial\boldsymbol{x}}\dot{\boldsymbol{x}} = \boldsymbol{J}\boldsymbol{\Phi}(\boldsymbol{x}) \tag{16}$$

where

$$\boldsymbol{\Phi}(\boldsymbol{x}) = \begin{bmatrix} \phi_1 \\ \phi_2 \end{bmatrix} = \begin{bmatrix} (U - ri_{\rm L} - u_{\rm C})/L \\ (i_{\rm L} - P_{\rm e}/u_{\rm C})/C \end{bmatrix}. \tag{17}$$

The Lyapunov function can be constructed as follows:

$$\mathbf{V}(\boldsymbol{x}) = \dot{\boldsymbol{x}}^{\rm T}\boldsymbol{H}\dot{\boldsymbol{x}} = \boldsymbol{\Phi}(\boldsymbol{x})^{\rm T}\boldsymbol{H}\boldsymbol{\Phi}(\boldsymbol{x}) \tag{18}$$

where $\boldsymbol{H}$ is positive definite, hence $\boldsymbol{V}(\boldsymbol{x})$ is also positive definite. The full derivative of $\boldsymbol{V}(\boldsymbol{x})$ for t is calculated as follows:

$$\dot{\boldsymbol{V}}(\boldsymbol{x}) = -\boldsymbol{\Phi}(\boldsymbol{x})^{\rm T}\boldsymbol{Q}(\boldsymbol{x})\boldsymbol{\Phi}(\boldsymbol{x}) \tag{19}$$

and

$$\boldsymbol{Q}(\boldsymbol{x}) = -[\boldsymbol{J}^{\rm T}\boldsymbol{H} + \boldsymbol{H}\boldsymbol{J}]. \tag{20}$$

In order to ensure the progressive stability of the system under small disturbance, the negative definiteness of $\dot{\mathbf{V}}(\boldsymbol{x})$must be guaranteed. Therefore, set $\boldsymbol{Q}(\boldsymbol{x}) = \boldsymbol{I}$, then $\boldsymbol{H}$ can be derived as follows:

$$\boldsymbol{H} = \begin{bmatrix} h_{\rm a} & h_{\rm b} \\ h_{\rm b} & h_{\rm c} \end{bmatrix} = \frac{\mathbf{I} + \det(\boldsymbol{J})(\boldsymbol{J}\boldsymbol{J}^{\rm T})^{-1}}{-2Tr(\boldsymbol{J})} \tag{21}$$

where det($\boldsymbol{J}$) is the determinant of $\boldsymbol{J}$, $Tr(\boldsymbol{J})$ is the trace of $\boldsymbol{J}$, and $\boldsymbol{I}$ is the unit matrix. The symbolic expression of $\boldsymbol{H}$ can be seen in (55)–(57) in the Appendix.

To ensure positive definiteness of $\boldsymbol{H}$, it should be satisfied

$$\begin{cases} \Delta_1 = h_{\rm a} > 0 \\ \Delta_2 = h_{\rm a}h_{\rm c} - h_{\rm b}^2 > 0 \end{cases} \tag{22}$$

which means

$$\begin{cases} rP_{\rm e} - u_{\rm C}^2 < 0 \\ LP_{\rm e} - Cu_{\rm C}^2 r < 0 \end{cases}. \tag{23}$$

That is, under the condition of (23), the system is of small-signal stability.

To further verify the stability of system under large disturbance, $\boldsymbol{H}$ is rewritten as follows:

$$\boldsymbol{H} = \begin{bmatrix} h_{\rm a0} + h_{\rm a1} & h_{\rm b} \\ h_{\rm b} & h_{\rm c0} + h_{\rm c1} \end{bmatrix}. \tag{24}$$

It can be seen from (22) and (24) that there is $h_{\rm a0}h_{\rm c0} = {h_{\rm b}}^2$ and $\min\{h_{\rm a0}, h_{\rm a1}, h_{\rm c0}, h_{\rm c1}\}\geq 0$ existing simultaneously. Therefore, $\boldsymbol{V}(\boldsymbol{x})$ can be expressed as follows:

$$\begin{aligned} \mathbf{V}(\boldsymbol{x}) &= h_{\rm a}\phi_1^2 + 2h_{\rm b}\phi_1\phi_2 + h_{\rm c}\phi_2^2 \\ &= (\sqrt{h_{\rm a0}}\phi_1 + \sqrt{h_{\rm c0}}\phi_2)^2 + h_{\rm a1}\phi_1^2 + h_{\rm c1}\phi_2^2. \end{aligned} \tag{25}$$

Obviously, when $\|\boldsymbol{x}\|\to\infty$, $\boldsymbol{V}(\boldsymbol{x})\to\infty$ will be satisfied. This means, under the condition of (23), the system is of large-signal stability.

B. Supplementary Explanation of Sufficiency and Necessity

The shortcoming of the Lyapunov direct method is conservatism. In other words, it can only explain the sufficiency of (23) and cannot explain its necessity. Here, we give its necessity as follows.

For the second-order system given by (14), the necessary and sufficient criterion for small-signal stability is as follows:

$$\begin{cases} \mathrm{Tr}(\boldsymbol{J}) < 0 \\ |\boldsymbol{J}| > 0 \end{cases} \tag{26}$$

which can be simplified as follows:

$$\begin{cases} rP < u_{\mathrm{C}}^2 \\ LP < Cu_{\mathrm{C}}^2 r. \end{cases} \tag{27}$$

It is obvious that (27) is the transformation of (23), which means (23) is also the necessary and sufficient criterion for small-signal stability. In addition, if a system is of large-signal stability, it must first be of small-signal stability. Hence, formula (23) is both necessary and sufficient criterion for large-signal stability. The second subformula of (23) can be also derived by MPT, but the first one cannot. The detailed comparisons are shown in the following content.

C. Comparisons With MPT

From the law of MPT [30] [detailed in (58)–(60) in the Appendix], the mixed potential function in this article can be constructed as follows:

$$P\left(i_L, u_C\right) = -\frac{1}{2} r i_L^2 + \int_0^{u_C} \frac{P_e}{u_C} du_C + i_L\left(U_{\mathrm{rate}} - u_C\right) \tag{28}$$

where $A(i_L) = \frac{1}{2} r i_L^2, B(u_C) = \int_0^{u_C} \frac{P_e}{u_C} du_C, (i, \gamma v - \alpha) = i_L(U_{\mathrm{rate}} - u_C)$, $A_{ii}(i) = \frac{\partial^2 A(i_L)}{\partial i_L^2} = r$, and $B_{vv}(u_C) = \frac{\partial^2 B(u_C)}{\partial u_C^2} = \frac{-P_e}{u_C^2}$.

Defining μ_1 the minimum eigenvalue of matrix $L^{-1/2} A_{ii}(i_L) L^{1/2}$, μ_2 the minimum eigenvalue of matrix $C^{-1/2} B_{vv}(u_C) C^{1/2}$, μ_1 and μ_2 can be calculated as follows:

$$\mu_1 = \frac{r}{L}, \mu_2 = \frac{-P_e}{Cu_C^2}. \tag{29}$$

To make the system stable, it should first satisfy the following:

$$\mu_1 + \mu_2 = \frac{r}{L} - \frac{P_e}{Cu_C^2} > 0 \Rightarrow LP_{\mathrm{e}} - Cu_{\mathrm{C}}^2 r < 0 \tag{30}$$

which is the same as the second subformula of (23). Second, it should simultaneously satisfy when $|i_L| + |u_C| \to \infty$, $P^*(i_L, u_C) \to \infty$. In this article, $P^*(i_L, u_C)$ is expressed as follows:

$$\begin{aligned} P^*\left(i_L, u_C\right) = & \frac{1}{2}\left(\frac{r}{L} + \frac{P_e}{Cu_C^2}\right) \\ & \times \left(-\frac{1}{2} r i_L^2 + \int_0^{u_C} \frac{P_e}{u_C} du_C + i_L\left(U_{\mathrm{rate}} - u_C\right)\right) \\ & + \frac{1}{2L}\left(-r i_L + U - u_C\right)^2 + \frac{1}{2C}\left(\frac{P_e}{u_C} - i_L\right)^2. \end{aligned}$$

When $|i_L| + |u_C| \to \infty$, $P^*(i_L, u_C)$ can be simplified as follows:

$$P^*\left(i_L, u_C\right) = \underbrace{\frac{i_L^2}{2}\left(\frac{1}{C} + \frac{r^2}{2L}\right)}_{\infty} + \underbrace{\frac{-r}{4L} i_L u_C}_{-\infty}. \tag{31}$$

It not easy to rigidly judge $P^*(i_L, u_C) \to \infty$.

TABLE I
COMPARISONS BETWEEN TWO METHODS

Compared items	MPT	Lyapunov direct method
Criterion	$LP_{\mathrm{e}} - Cu_{\mathrm{C}}^2 r < 0$	$\begin{cases} rP_{\mathrm{e}} - u_{\mathrm{C}}^2 < 0 \\ LP_{\mathrm{e}} - Cu_{\mathrm{C}}^2 r < 0 \end{cases}$, more comprehensive
Derivation process	Not rigid	Perfectly rigid

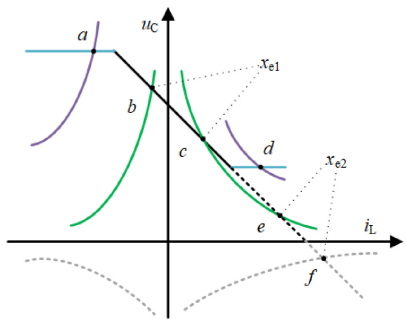

Fig. 4. Distribution of dc microgrid equilibrium points.

Hence, compared with the Lyapunov direct method, MPT is more difficult when using in this article, and the criterion is not as comprehensive as (23) because it cannot derive the first subformula of (23), but the first one is necessary and illustrated as (47). Therefore, (23) is taken as the stability criterion in this article. The comparisons are listed in Table I.

IV. Stability Analysis and Physical Interpretation

The studied system is of large-signal stability under the condition of (23), but more than one equilibrium point exists in mathematical solutions, as shown in Fig. 4. Due to the droop control characteristics, the output current of the energy storage system is a linear function of the bus voltage, whose slope is r and the intercept is U_{rate}, as shown by the straight line. The equivalent CPLs can be positive or negative, and the load current is inversely proportional to the bus voltage. If the equivalent CPLs are positive, the power curve and the droop control curve will intersect in the first quadrant. Otherwise, if the equivalent power load is negative, the two curves will intersect in the second and fourth quadrants. However, since the bus voltage cannot be negative, the intersection of the fourth quadrant will be ignored. Thus, only the stability of the upper half-plane equilibrium points (i.e., *a*, *b*, *c*, *d*, *e* shown in Fig. 4) will be discussed.

The equilibrium points of the system can be derived as follows:

$$\begin{cases} \boldsymbol{x}_{\mathrm{e1}} = \left[\, i_{\mathrm{Le1}} \; u_{\mathrm{Ce1}} \,\right] = \left[\, P_{\mathrm{e}}/u_{\mathrm{Ce1}} \; (U + w)/2 \,\right] \\ \boldsymbol{x}_{\mathrm{e2}} = \left[\, i_{\mathrm{Le2}} \; u_{\mathrm{Ce2}} \,\right] = \left[\, P_{\mathrm{e}}/u_{\mathrm{Ce2}} \; (U - w)/2 \,\right] \end{cases} \tag{32}$$

where

$$\begin{cases} w = \sqrt{U^2 - 4rP_{\mathrm{e}}} \\ P_{\mathrm{e}} < U^2/(4r) = P_{\max}. \end{cases} \tag{33}$$

It can be easily known from the derivation process that a, b, c, and $d \in x_{e1}$, whereas $e \in x_{e2}$.

For the convenience of analysis, formula (27) is rewritten as follows:

$$P_e < r^2 C/L \cdot (u_C^2/r) \tag{34}$$

and

$$P_e < u_C^2/r. \tag{35}$$

That is, if the system is to maintain the large-signal stability, it must satisfy both (34) and (35) simultaneously.

From (34) and (35), it is obvious when $P_e < 0$, the system is always in a stable state, which means points a and b are always in the stable state. On the other hand, when $P_e > 0$, the stability of the system cannot be directly seen. From Section II, in the second stage, r is infinitely close to 0. However, in a practical microgrid system, considering the resistance of lines and other devices, r will not completely be zero. Besides, c and $d \in x_{e1}$, thus the stability constraint of point d should be consistent with c. Thus, only stability of point c and e will be analyzed below.

A. Stability Analysis of Point c

From (34) and (35), it can be seen when $L < r^2 C$, x_{e1} only needs to satisfy (35). Substituting x_{e1} into (35) and making simplification, it can be derived as follows:

$$w^2 + U_{rate} w > 0. \tag{36}$$

Obviously, under the condition of (33), (36) is always satisfied. That is, when $L < r^2 C$, for $\forall P_e < P_{max}$, the system is always stable.

On the other hand, when $L > r^2 C$, x_{e1} only needs to satisfy (34). Substituting x_{e1} into (30), it can be simplified as follows:

$$(2L + 2r^2 C)/(rC) \cdot P_e - U_{rate}^2 < U_{rate} w. \tag{37}$$

If the equivalent CPLs satisfy

$$P_e < \frac{2r^2 C}{L + r^2 C} \cdot P_{max} \tag{38}$$

then (37) will always be satisfied. Otherwise, P_e needs to satisfy

$$\frac{2r^2 C}{L + r^2 C} \cdot P_{max} < P_e < \frac{2r^2 C}{L + r^2 C} \cdot \frac{2L}{L + r^2 C} \cdot P_{max}. \tag{39}$$

Particularly, it is easy to prove that

$$2L/(L + r^2 C) > 1. \tag{40}$$

Hence, the inequality relationship of (39) is correctly established.

In summary, when $L > r^2 C$, the system is of large-signal stability under the condition of

$$P_e < 4r^2 CL \Big/ (L + r^2 C)^2 \cdot P_{max} = P'_{max}. \tag{41}$$

B. Stability Analysis of Point e

When $L < r^2 C$, x_{e2} only needs to satisfy (35). Substitute x_{e2} into (35) and it can be simplified as follows:

$$w\,(w - U_{rate}) > 0. \tag{42}$$

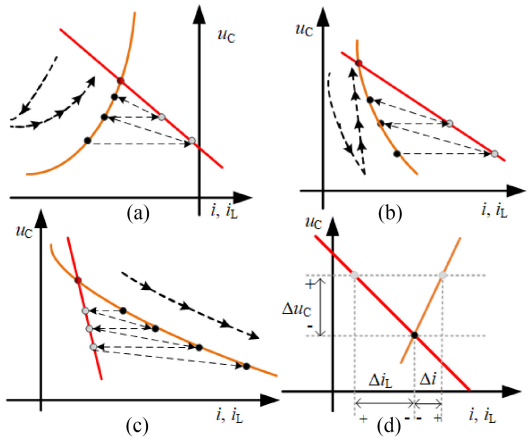

Fig. 5. Schematic diagram of physical interpretation of large signal stability. (a) First type. (b) Second type. (c) Third type. (d) Physical process of stability.

Obviously, for $\forall P_e > 0$, formula (42) would never be satisfied.

On the other hand, when $L > r^2 C$, x_{e2} can automatically satisfy (34). However, for $\forall P_e > 0$, formula (42) would never be satisfied. Hence, the system is unstable at point e.

C. Physical Interpretation of Equilibrium Points

To summarize the above analysis, equilibrium points of dc microgrids can be divided into three types, as shown in Fig. 5, where point a and b are classified into the first type, point c and d are classified into the second type, and point e is classified into the third type.

1) *The first type:* The equilibrium point in Fig. 5(a) shows the characteristics of $P_e < 0$. Assuming the system is in steady-state at this point, if any disturbance occurs at the same time, the bus voltage will have a disturbance increment. If the increment is negative, the current from negative power load to the dc bus will increase according to the power curve but is simultaneously larger than the current needed by droop control, that is i–$i_L < 0$. At this time, the extra current will flow into the parallel capacitor causing the bus voltage to rise. Otherwise, if the increment is positive, the physical process will be similar. Hence, the system is of large-signal stability when operating at points of this type. From Fig. 5(a), mathematical description of the first type can be derived as follows:

$$\frac{di_L}{du_C} < 0 < \frac{di}{du_C}, i_{Le} < 0. \tag{43}$$

2) *The second type:* The equilibrium point in Fig. 5(b) shows the characteristics of $P_e > 0$. Assuming the system is in steady-state at this point, and if any disturbance occurs at this time, the bus voltage will have a disturbance increment. If the increment is negative, the needed load current will increase but is still smaller than the output current by droop control, that is i–$i_L < 0$, the extra current will flow into the parallel capacitor bringing about the rise of the bus voltage. Otherwise, if the increment is positive,

the physical process will be similar. Hence, the system is of large-signal stability when operating at points of this type. From Fig. 5(b), the mathematical description of the second type can be derived as follows:

$$\frac{di_{\mathrm{L}}}{du_{\mathrm{C}}} < \frac{di}{du_{\mathrm{C}}} < 0, i_{\mathrm{Le}} > 0. \tag{44}$$

3) *The third type:* The equilibrium point in Fig. 5(c) is not of large-signal stability, analyzed as follows. Assuming the system is in steady-state at this point, and if any disturbance occurs at this time, the bus voltage will have a disturbance increment. If the increment is negative, the needed load current will increase and is unfortunately larger than the output current by droop control, that is, i–$i_{\mathrm{L}} > 0$. The capacitor will discharge to make up the discrepancy leading to a further decline of the bus voltage. Otherwise, if the increment is positive, the physical process will be similar. Hence, the system is not of large-signal stability when operating at points of this type. The mathematical description of the second type can be derived as follows:

$$\frac{di}{du_{\mathrm{C}}} < \frac{di_{\mathrm{L}}}{du_{\mathrm{C}}} < 0, i_{\mathrm{Le}} > 0. \tag{45}$$

4) *Summary:* Through the analysis of the above physical process, it can be found that the essence of the first and second type is that the polarity of bus voltage change is opposite to the polarity of the current change flowing into the capacitor. In other words, the control process can make up the bus voltage disturbance increment, as shown in Fig. 5(d). Thus, the mathematical model can be expressed as follows:

$$\Delta u_{\mathrm{C}} \cdot (\Delta i_{\mathrm{L}} - \Delta i) < 0 \tag{46}$$

which can be rewritten as follows:

$$\frac{di_{\mathrm{L}}}{du_{\mathrm{C}}} < \frac{di}{du_{\mathrm{C}}} \Rightarrow rP_{\mathrm{e}} - u_{\mathrm{C}}^2 < 0. \tag{47}$$

It is consistent with (43) and (44).

The above analysis figures out the necessary criterion of stability from the aspects of control process and physical meaning, but is not of sufficiency. The effect of the physical parameters such as L and C of the system itself on stability should still be considered, so that the second subformula in (23) should be also satisfied.

V. Stability Domain of Power Load Limit

As analyzed in Section IV, the reason for system instability under different parameters is that the equivalent constant power load P_{e} is greater than the maximum load power allowed by the system under a certain circumstance. In this sense, it is necessary to calculate the power load limit that the system can carry under different conditions, which is also meaningful in dc microgrids' energy management.

A. Theoretical Analysis of Power Limit

Considering the circumstance that $P_{\mathrm{e}} > 0$, the maximum power load P_{lim1} that the system can carry under different parameter groups can be calculated as follows:

$$\begin{cases} P_{\mathrm{lim1}} = \begin{cases} P'_{\max} & r < r_0 \\ P_{\max} & r > r_0 \end{cases} \\ r_0 = \sqrt{L/C}. \end{cases} \tag{48}$$

That is, under different parameter groups, the stability criterion is $P_{\mathrm{e}} < P_{\mathrm{lim1}}$. Therefore, once the L, C, and r parameters are fixed, the value of P_{e} directly determines the stability of the system under stability constraint.

It can be seen from (48), when $r > r_0$, P_{lim1} monotonically decreases as r increases; when $r < r_0$, the trend of P_{lim1} with r cannot be visually seen. Hence, defining

$$\Psi(r) = \frac{4r^2CL}{(L + r^2C)^2} \cdot \frac{U^2}{4r} \tag{49}$$

the first derivative of (49) is as follows:

$$\dot{\Psi}(r) = \frac{CLU^2}{(L + r^2C)^2} \cdot \frac{L - 3r^2C}{L + r^2C}. \tag{50}$$

It can be seen that P_{lim1} gets the maximum value when $r = r_0/\sqrt{3}$. Defining the maximum point as $T(r_{\mathrm{T}}, P_{\mathrm{T}})$, where $r_{\mathrm{T}} = r_0/\sqrt{3}$, stability margin M_P can be defined as follows:

$$M_P = (P_{\mathrm{T}} - P_{\mathrm{e}})/P_{\mathrm{T}}. \tag{51}$$

Furthermore, the nonlinear region $[\mathrm{B}_{k,1}, \mathrm{A}_{k,1}]$ is a constant stable region, but $[\mathrm{A}_{k,2}, \mathrm{B}_{k,2}]$ is an unstable region under ideal conditions. Hence, the system should not operate in the nonlinear region as much as possible. Taking the first quadrant as an example, for a certain r, the bus voltage gradually decreases as P_{e} increases. Assuming the allowed voltage deviation range is $[\delta_1 U_{\mathrm{rate}}, \delta_2 U_{\mathrm{rate}}]$, then the allowed maximum power load is as follows:

$$P_{\mathrm{lim2}} = \delta_i(1 - \delta_i)U_{\mathrm{rate}}^2/r, i = 1, 2 \tag{52}$$

where δ_1 and δ_2 are, respectively, the upper and lower deviation limits of the bus voltage separately, and CPLs must satisfy $P_{\mathrm{e}} < |P_{\mathrm{lim2}}|$.

Hence, the power limit P_{lim} constrained by the large-signal stability and voltage deviation should be the smaller one between P_{lim1} and $|P_{\mathrm{lim2}}|$, that is

$$P_{\mathrm{lim}} = \min\{P_{\mathrm{lim1}}, |P_{\mathrm{lim2}}|\}. \tag{53}$$

B. Case Study

A study case is conducted to illustrate the power limit calculation, where parameters are set in Table II, and constraints are calculated in Table III. Fig. 6 shows the simulation results of C being set as 25 mF. Assuming the intersection point of curve P_{lim2} and curve P_{lim1} is $Q(r_{\mathrm{Q}}, P_{\mathrm{Q}})$, it can be seen

$$P_{\mathrm{lim}} = \begin{cases} P_{\mathrm{lim2}}, P_{\mathrm{e}} < 0 \\ P_{\mathrm{lim\,1}}, r < r_{\mathrm{Q}} \text{ and } P_{\mathrm{e}} > 0 \\ P_{\mathrm{lim2}}, r \geq r_{\mathrm{Q}} \text{ and } P_{\mathrm{e}} > 0 \end{cases} \tag{54}$$

where P_{lim} is shown as the pink area in Fig. 6.

TABLE II
PHYSICAL PARAMETERS FOR SIMULATION

Symbol	Description	Value
U_{rate}	rated voltage	200 V
δ_1, δ_2	lower and upper limits of voltage deviation	0.9, 1.1 p.u.
r	equivalent virtual resistance	0.048Ω
L	equivalent output inductance	0.05mH
C	equivalent capacitance	25mF, 6mF

TABLE III
PARAMETERS CONSTRAINS FOR SIMULATION

Condition	C	P_{lim1}	P_{lim2}	r_Q
$L<r^2C$	25mF	0.21MW	0.07MW, as $P_e>0$	0.015Ω
$L>r^2C$	6mF	0.14MW	-0.09MW, as $P_e<0$	0.031Ω

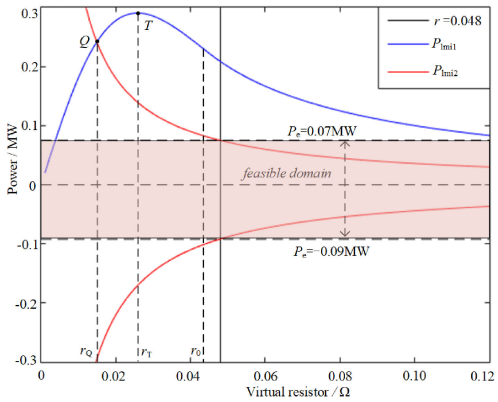

Fig. 6. Feasible domain of CPL with stability and voltage deviation constraints.

1) *Under the condition of* $L < r^2C$*:* Fig. 7 shows the waveforms of $C = 25$ mF ($L < r^2C$). It can be seen from Fig. 7(a) that when $P_e < 0$, the system can converge stably. The waveform of x_{e1} when $P_e > 0$ is shown in Fig. 7(b), where it can be seen if $P_e < P_{lim1}$, the system can converge steadily. However, the convergence speed will be gradually slowed down as P_e increases. To be emphasized, when $P_e = 0.22$ MW $> P_{lim1}$, the system cannot converge any more.

From Fig. 7(a) and (b), it also can be concluded that, when $P_e < |P_{lim2}|$, dc voltage can satisfy deviation requirements, otherwise it cannot. Specifically, when $P_e = –0.10$ MW $< P_{lim2}$ in Fig. 7(a), the dc voltage will be larger than 220 V; when $P_e = 0.10$ MW $> P_{lim2}$ in Fig. 7(b), the voltage will be lower than 180 V. The characteristics shown in Fig. 7(a) and (b) are consistent with the theoretical analysis.

2) *Under the condition of* $L > r^2C$*:* A case under the condition of $L > r^2C$ is also conducted, as shown in Fig. 8, where the capacitance parameter is modified to 6 mF, the other parameters remain unchanged.

The waveforms of $P_e < 0$ are shown in Fig. 8(a), and the system can converge stably. The waveforms of $P_e > 0$ are shown in Fig. 8(b), where the system can converge stably when $P_e < P_{lim1}$, whereas the system cannot converge when $P_e > P_{lim1}$.

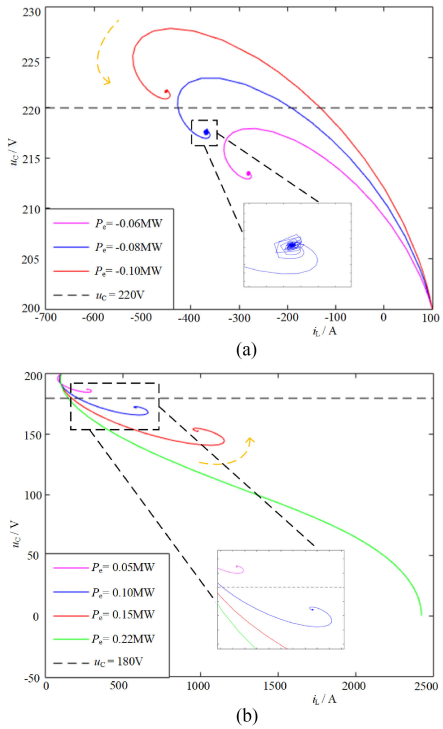

Fig. 7. Simulation waveforms under the condition of $L < r^2C$. (a) Simulation waveforms when $P_e < 0$. (b) Simulation waveforms when $P_e > 0$.

Specifically, when $P_e = –0.10$ MW $< P_{lim2}$ in Fig. 8(a), dc voltage will be larger than 220 V; when $P_e > P_{lim2}$ ($P_e = 0.08$ MW and $P_e = 0.12$ MW) in Fig. 8(b), dc voltage will be lower than 180 V, although the system is stable; when $P_e = 0.16$ MW $> P_{lim1}$, the system cannot converge stably. These results are consistent with the theoretical analysis.

VI. SIMULATION AND EXPERIMENTAL RESULTS

From the analysis of Section IV, point *a* and *b* are always stable, point *e* is always unstable, and the stability of points *c* and *d* are influenced by system parameters, stability boundary of them are shown in (49). Considering the requirements of voltage derivation, the power boundary will be changed to be (53). Both boundaries will be verified separately in this part.

An experimental islanded dc microgrid setup, shown in Fig. 9(a) and (b), was used to verify the power load limits under large-signal stability and voltage deviation constraints. The setup consists of a dc source, four parallel-connected dc/dc converters (GCs), *LC* filters, electronic loads (CPLs), and dSPACE controller as well as its monitoring platform. The experimental parameters are shown in Table IV, and the power load limit in the experimental study-cases is analyzed, as shown in Fig. 9(c) and listed in Table V. Besides, simulations with the same structure and parameters are conducted to make comparisons, as shown in Tables VI and VII. From (41), the power load limits may be influenced by parasitic parameters of the experimental setup. But there is no obvious difference between simulation and experimental results, because the parasitic parameters are small enough compared to *LC* filter.

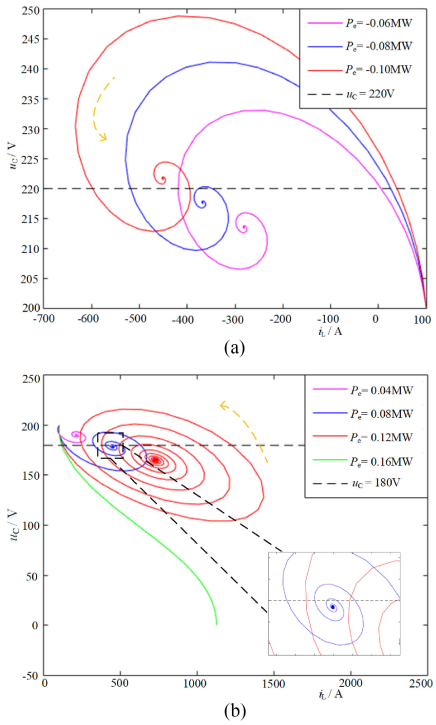

Fig. 8. Simulation waveforms under the condition of $L > r^2C$. (a) Simulation waveforms when $P_e < 0$. (b) Simulation waveforms when $P_e > 0$.

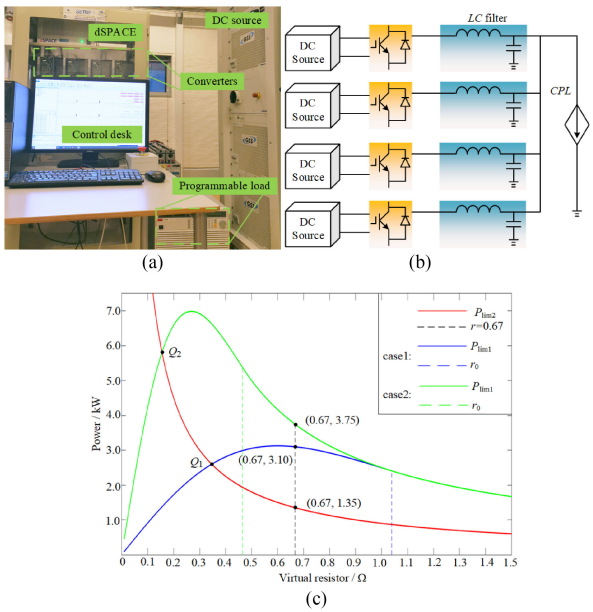

Fig. 9. Experimental platform and cases analysis. (a) Experimental setup in AAU-MG research laboratory. (b) Circuit diagram of testing setup. (c) Power limit analysis of experimental cases.

A. Case 1: Verification for $L > r^2C$

Fig. 10 shows the waveforms of simulation and experimental verifications, where equivalent capacitance value fixed at $C = 0.5$ mF, and the parameters P_{lim1}, P_{lim2}, and r_{Q} calculated as shown in Table V, where $r > r_{\text{Q}}$. The simulation results are shown in Fig. 10(a)–(c), where 1, 1.5, 2.5, and 3.3 kW CPLs are connected to the dc microgrid at $t = 0.025$ s, $t = 0.05$ s, $t = 0.075$ s, and $t = 0.1$ s, respectively. The dc voltage during different time stages is listed in Table VI. It can be seen that when $P_{\text{e}} < P_{\text{lim2}}$, the bus voltage can satisfy both constraints; when $P_{\text{lim2}} < P_{\text{e}} < P_{\text{lim1}}$, the bus voltage can only satisfy stability constraint; when $P_{\text{lim1}} < P_{\text{e}}$, the system is unstable.

In experimental verification, the same loads as those in simulation are connected to the dc microgrid at $t = T_1$, $t = T_2$, $t = T_3$, and $t = T_4$, respectively, and the experimental waveforms are shown in Fig. 10(d)–(f). The detailed information is also listed in Table VI, and the same conclusions as those in simulation results can be concluded. The difference is that at

TABLE IV
PHYSICAL PARAMETERS FOR EXPERIMENT

Converters	Parameters		Equivalent Parameters
GC_1	r_1=2Ω, L_4=2.2mH	case1:C_1=0.1mF case2:C_1=0.6mF	r=0.67Ω
GC_2	r_2=2Ω, L_4=2.3mH	case1:C_2=0.1mF case2:C_2=0.6mF	L=0.54mH
GC_3	r_3=4Ω, L_4=2.2mH	case1:C_3=0.1mF case2:C_3=0.6mF	case1:C=0.5mF
GC_4	r_4=4Ω, L_4=2.0mH	case1:C_4=0.2mF case2:C_4=0.7mF	case2:C=2.5mF

TABLE V
PARAMETERS CONSTRAINS FOR EXPERIMENT

Conditions	P_{lim1}	P_{lim2}	r_{Q}	Voltage
case1: $L>r^2C$	3.10kW	1.35kW	0.35Ω	U_{rate}=100V δ_1=0.9p.u. δ_2=1.1p.u.
case2: $L<r^2C$	3.75kW	1.35kW	0.16Ω	

TABLE VI
VERIFICATION RESULTS OF CASE 1

Time stages	Load conditions	Voltage states
0.025s~0.05s (T_1~T_2)	1.0kW< P_{lim2}	Stable, and u_C>90V.
0.05s~0.075s (T_2~T_3)	P_{lim2}<1.5kW< P_{lim1}	Stable, but u_C<90V.
0.75s~0.1s (T_3~T_4)	P_{lim2}<2.5kW< P_{lim1}	Stable, but u_C<90V.
0.1s~0.15s (T_4~)	P_{lim1}<3.3kW	Not stable.

TABLE VII
VERIFICATION RESULTS OF CASE 2

Time stages	Load conditions	Voltage states
0.025s~0.05s (T_5~T_6)	1.0kW< P_{lim2}	Stable, and u_C>90V.
0.05s~0.075s (T_6~T_7)	P_{lim2}<1.5kW< P_{lim1}	Stable, but u_C<90V.
0.75s~0.1s (T_7~T_8)	P_{lim2}<2.5kW< P_{lim1}	Stable, but u_C<90V.
0.1s~0.125s (T_8~T_9)	P_{lim2}<3.5kW< P_{lim1}	Stable, but u_C<90V
0.125s~0.16s (T_9~)	P_{lim1}<3.8kW	Not stable.

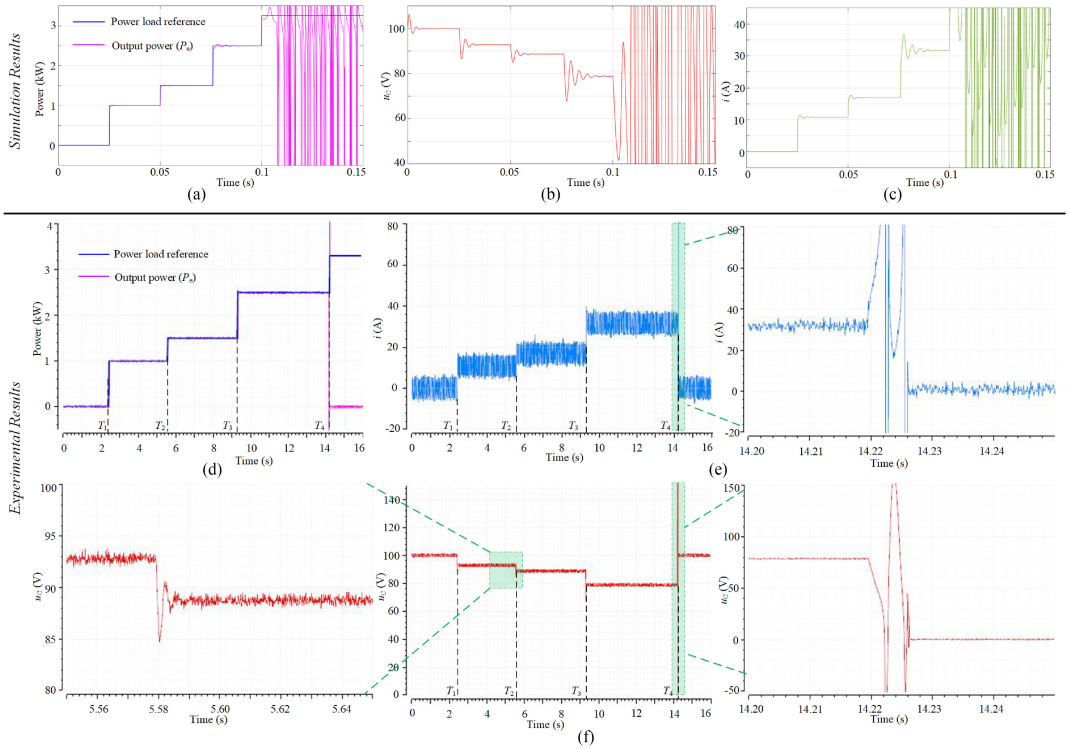

Fig. 10. Simulation and experimental waveforms under the condition of $L > r^2C$. (a)Simulation waveforms of power load and its reference. (b) Simulation waveforms of current of load. (c) Simulation waveforms of dc bus voltage. (d) Experimental waveforms of power load and its reference. (e) Experimental waveforms of current of load. (f) Experimental waveforms of dc bus voltage.

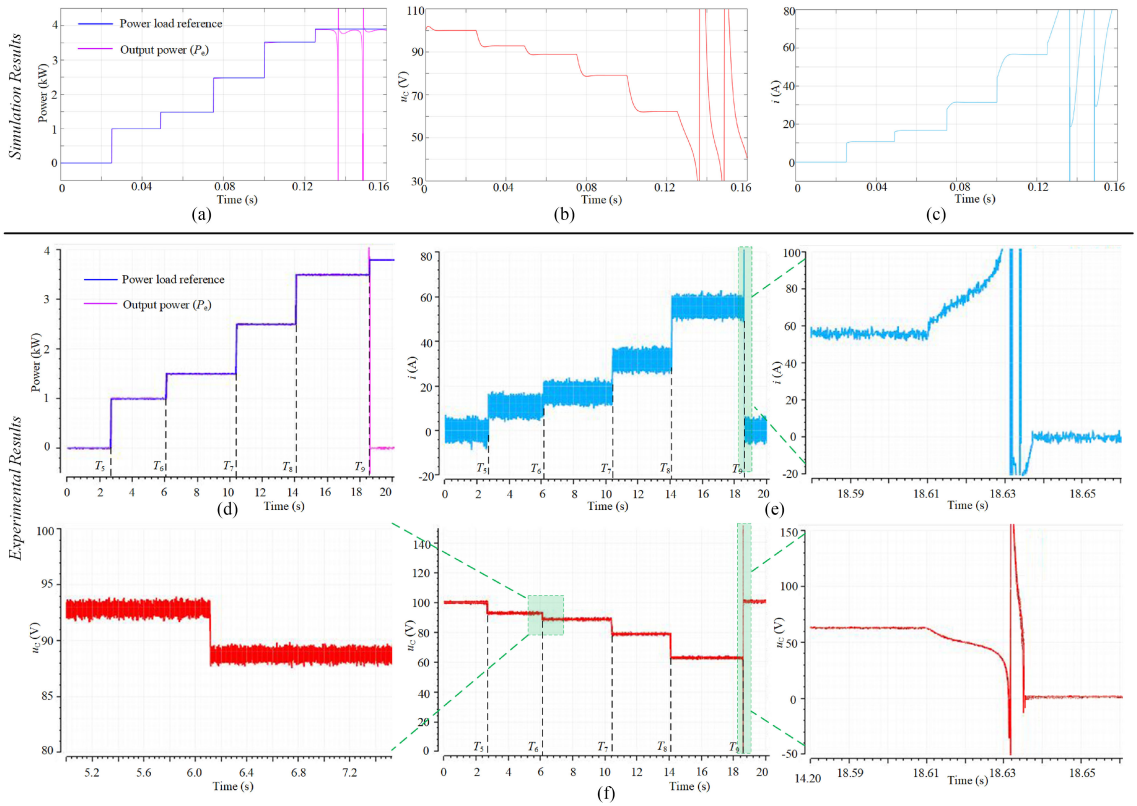

Fig. 11. Simulation and experimental waveforms under the condition of $L < r^2C$. (a) Simulation waveforms of power load and its reference. (b) Simulation waveforms of current of load. (c) Simulation waveforms of dc bus voltage. (d) Experimental waveforms of power load and its reference. (e) Experimental waveforms of current of load. (f) Experimental waveforms of dc bus voltage.

$t = T_4$ because CPLs are larger than the power limit $P_{\lim 1}$, the system becomes divergent, resulting in the huge transient current triggering protections, and then the current turns zero, and bus voltage goes back to its nominal value.

B. Case 2: Verification for $L < r2C$

In this case, the equivalent capacitance value is fixed at $C = 2.5$ mF to satisfy $L < r^2C$, and constraints are calculated in Table V, where $r > r_{\mathrm{Q}}$. The simulation results are shown in Fig. 11(a)–(c), where 1, 1.5, 2.5, 3.5, and 3.8 kW CPLs are connected to the dc microgrid at $t = 0.025$ s, $t = 0.05$ s, $t = 0.075$ s, $t = 0.1$ s, and $t = 0.125$ s, respectively. The dc voltage during different time stages is listed in Table VII. It can be seen that when $P_{\mathrm{e}} < P_{\lim 2}$, the bus voltage can satisfy both constraints; when $P_{\lim 2} < P_{\mathrm{e}} < P_{\lim 1}$, the bus voltage can only satisfy stability constraint; when $P_{\lim 1} < P_{\mathrm{e}}$, the system is unstable.

In experimental verification, the same loads as those in simulation are connected to the dc microgrid at $t = T_5$, $t = T_6$, $t = T_7$, $t = T_8$, and $t = T_9$, respectively, and the experimental waveforms are shown in Fig. 11(d)–(f). The detailed information is also listed in Table VII, and the same conclusions as those in simulation results can be concluded. The difference is that, at $t = T_9$, the system becomes divergent and the huge transient current triggers protections, leading to the consequences of current turning to be zero and bus voltage going back to its nominal value.

Summing up, we can observe that the experimental results are consistent with the theoretical analysis previously done.

VII. Conclusion

This article presents a large-signal stability analysis from the system-level perspective. First, the normalized equivalent model of a droop-controlled dc microgrid under different operation stages with multiple parallel-connected GCs is proposed. Then, the model is used for the large-signal stability analysis purpose by using the Lyapunov direct method, and the stability criterion is derived mathematically achieving conservatism-free. Besides, the MPT method is used to make comparisons with the Lyapunov direct method to enhance the advantages of the latter. Based on the derived criterion, stability of equilibrium points is discussed and its physical interpretation is first explored. Finally, the power load limit is calculated within both constraints of stability and voltage deviations. The load limit calculation is proposed to be expanded in the future of energy management systems. However, there are still some shortages in this article that the stability criterion is only suitable for a dc microgrid adopting droop control or voltage constant strategy, and all GCs must be centrally arranged.

Appendix

The symbolic expression of $\boldsymbol{H}$ can be expressed as follows:

$$h_{\mathrm{a}} = (L(Cu_{\mathrm{C}}^4 + LP_{\mathrm{e}}^2 + Lu_{\mathrm{C}}^4) - CLP_{\mathrm{e}}u_{\mathrm{C}}^2 r)/ (2(LP_{\mathrm{e}} - Cu_{\mathrm{C}}^2 r)(P_{\mathrm{e}} r - u_{\mathrm{C}}^2)) \tag{55}$$

$$h_{\mathrm{b}} = CLu_{\mathrm{C}}^2(ru_{\mathrm{C}}^2 + P_{\mathrm{e}})/(2(LP_{\mathrm{e}} - Cu_{\mathrm{C}}^2 r)(P_{\mathrm{e}} r - u_{\mathrm{C}}^2)) \tag{56}$$

and

$$h_{\mathrm{c}} = Cu_{\mathrm{C}}^2(Cu_{\mathrm{C}}^2 + Lu_{\mathrm{C}}^2 + Cu_{\mathrm{C}}^2 r^2 - LP_{\mathrm{e}} r)/ (2(LP_{\mathrm{e}} - Cu_{\mathrm{C}}^2 r)(P_{\mathrm{e}} r - u_{\mathrm{C}}^2)). \tag{57}$$

The principle of MPT is detailed as follows. For a nonlinear circuit, its mixed potential function can be constructed as follows:

$$P(i, v) = -A(i) + B(v) + (i, \gamma v - \alpha) \tag{58}$$

where i is the inductor current, u is the capacitor voltage, $A(i)$ represents the current potential function, $B(v)$ represents the voltage potential function, γ represents the constant matrix associated with the structure, and α is a constant vector. Besides, it should satisfy

$$\begin{cases} L\frac{di}{dt} = \frac{\partial P(i,v)}{\partial i} \\ C\frac{dv}{dt} = \frac{\partial P(i,v)}{\partial v} \end{cases} \tag{59}$$

which can be used to verify the correctness of energy function.

To illustrate the stability analysis process, several variables need to be defined as follows:

$$\begin{cases} P_i = \frac{\partial P(i,v)}{\partial i}, P_v = \frac{\partial P(i,v)}{\partial v} \\ A_{ii}(i) = \frac{\partial^2 A(i)}{\partial i^2}, B_{vv}(v) = \frac{\partial^2 B(v)}{\partial v^2}. \end{cases} \tag{60}$$

Besides, let μ_1 represent the minimum eigenvalue of matrix $L^{-1/2}A_{ii}(i)\ L^{1/2}$, and μ_2 represent the minimum eigenvalue of matrix $C^{-1/2}B_{vv}(v)\ C^{1/2}$, where L and C are inductance matrix and capacitor matrix, respectively.

If a system is stable, it should satisfy the following two conditions. The first one is

$$\mu_1 + \mu_2 > 0. \tag{61}$$

The second one is, when $|i| + |v| \to \infty$

$$P^*(i, v) = \frac{\mu_1 - \mu_2}{2} P(i, v) + \frac{1}{2} P_i^T \left(L^{-1} P_i\right) + \frac{1}{2} P_v^T \left(C^{-1} P_v\right) \to \infty. \tag{62}$$

Then, the system can be considered as large-signal stable, and correspondingly, all solutions will gradually converge to the steady value.

In this article, the mixed potential function can be constructed as follows:

$$\begin{aligned} P(i_L, u_C) &= \int_0^{i_L} U_{\mathrm{rate}} di_L - \int_0^{i_L} r i_L di_L - \int_0^{i_e} u_C di_e \\ &\quad - \left(i_L - \frac{P_e}{u_C}\right) u_C \\ &= U_{\mathrm{rate}} i_L - \frac{1}{2} r i_L^2 - \left(u_C i_e - \int_0^{u_C} \frac{P_e}{u_C} du_C\right) \\ &\quad - i_L u_C + P_e, \\ &= -\frac{1}{2} r i_L^2 + \int_0^{u_C} \frac{P_e}{u_C} du_C + i_L (U_{\mathrm{rate}} - u_C) \end{aligned} \tag{63}$$

and detailed employment process is illustrated in Section III.

REFERENCES

[1] Y. Han, K. Zhang, H. Li, E. A. A. Coelho, and J. M. Guerrero, "MAS-based distributed coordinated control and optimization in microgrid and microgrid clusters: A comprehensive overview," *IEEE Trans. Power Electron.*, vol. 33, no. 8, pp. 6488–6508, Aug. 2018.

[2] N. Vafamand, M. H. Khooban, T. Dragičević, F. Blaabjerg, and J. Boudjadar, "Robust non-fragile fuzzy control of uncertain dc microgrids feeding constant power loads," *IEEE Trans. Power Electron.*, vol. 34, no. 11, pp. 11300–11308, Nov. 2019.

[3] M. Vahedipour-Dahraie, A. Anvari-Moghaddam, and J. M. Guerrero, "Evaluation of reliability in risk-constrained scheduling of autonomous microgrids with demand response and renewable resources," *IET Renewable Power Gener.*, vol. 12, no. 6, pp. 657–667, Apr. 2018.

[4] J. Lu, M. Savaghebi, Y. Guan, J. C. Vasquez, A. M. Y. M. Ghias, and J. M. Guerrero, "A reduced-order enhanced state observer control of dc-dc buck converter," *IEEE Access*, vol. 6, pp. 56184–56191, 2018.

[5] O. Cornea, G. Andreescu, N. Muntean, and D. Hulea, "Bidirectional power flow control in a dc microgrid through a switched-capacitor cell hybrid dc–dc converter," *IEEE Trans. Ind. Electron.*, vol. 64, no. 4, pp. 3012–3022, Apr. 2017.

[6] A. Kwasinski and C. N. Onwuchekwa, "Dynamic behavior and stabilization of DC microgrids with Instantaneous constant-power loads," *IEEE Trans. Power Electron.*, vol. 26, no. 3, pp. 822–834, Mar. 2011.

[7] R. Majumder, "Some aspects of stability in microgrids," *IEEE Trans. Power Syst.*, vol. 28, no. 3, pp. 3243–3252, Aug. 2013.

[8] N. Bottrell, M. Prodanovic, and T. C. Green, "Dynamic stability of a microgrid with an active load," *IEEE Trans. Power Electron.*, vol. 28, no. 11, pp. 5107–5119, Nov. 2013.

[9] F. Zhao, N. Li, Z. Yin, and X. Tang, "Small-signal modeling and stability analysis of DC microgrid with multiple type of loads," in *Proc. Int. Conf. Power Syst. Technol.*, 2014, pp. 3309–3315.

[10] X. Lu, K. Sun, J. M. Guerrero, J. C. Vasquez, L. Huang, and J. Wang, "Stability enhancement based on virtual impedance for dc microgrids with constant power loads," *IEEE Trans. Smart Grid*, vol. 6, no. 6, pp. 2770–2783, Nov. 2015.

[11] M. Kabalan, P. Singh, and D. Niebur, "Large signal lyapunov-based stability studies in microgrids: A review," *IEEE Trans. Smart Grid*, vol. 8, no. 5, pp. 2287–2295, Sep. 2017.

[12] A. Guha and G. Narayanan, "Small-signal stability analysis of an open-loop induction motor drive including the effect of inverter deadtime," *IEEE Trans. Ind. Appl.*, vol. 52, no. 1, pp. 242–253, Jan./Feb. 2016.

[13] F. Katiraei, M. R. Iravani, and P. W. Lehn, "Micro-grid autonomous operation during and subsequent to islanding process," *IEEE Trans. Power Del.*, vol. 20, no. 1, pp. 248–257, Jan. 2005.

[14] Z. Zhang, Q. Chen, R. Xie, and K. Sun, "The fault analysis of PV cable fault in dc microgrids," *IEEE Trans. Energy Convers.*, vol. 34, no. 1, pp. 486–496, Mar. 2019.

[15] J. Jiang *et al.*, "A conservatism-free large signal stability analysis method for dc microgrid based on mixed potential theory," *IEEE Trans. Power Electron.*, vol. 34, no. 11, pp. 11342–11351, Nov. 2019.

[16] P. Lin, C. Zhang, P. Wang, and J. Xiao, "A decentralized composite controller for unified voltage control with global system large-signal stability in dc microgrids," *IEEE Trans. Smart Grid*, vol. 10, no. 5, pp. 5075–5091, Sep. 2019.

[17] K. Wu, C. W. de Silva, and W. G. Dunford, "Stability analysis of isolated bidirectional dual active full-bridge dc–dc converter with triple phase-shift control," *IEEE Trans. Power Electron.*, vol. 27, no. 4, pp. 2007–2017, Apr. 2012.

[18] M. Kabalan, P. Singh and D. Niebur, "A design and optimization tool for inverter-based microgrids using large-signal nonlinear analysis," *IEEE Trans. Smart Grid*, vol. 10, no. 4, pp. 4566–4576, Jul. 2019

[19] M. Mokhtar, M. I. Marei, and A. A. El-Sattar, "An adaptive droop control scheme for dc microgrids integrating sliding mode voltage and current controlled boost converters," *IEEE Trans. Smart Grid*, vol. 10, no. 2, pp. 1685–1693, Mar. 2019.

[20] A. P. N. Tahim, D. J. Pagano, E. Lenz, and V. Stramosk, "Modeling and stability analysis of islanded dc microgrids under droop control," *IEEE Trans. Power Electron.*, vol. 30, no. 8, pp. 4597–4607, Aug. 2015.

[21] V. Nasirian, A. Davoudi, F. L. Lewis, and J. M. Guerrero, "Distributed adaptive droop control for dc distribution systems," *IEEE Trans. Energy Convers.*, vol. 29, no. 4, pp. 944–956, Dec. 2014.

[22] S. Peyghami, H. Mokhtari, P. C. Loh, P. Davari, and F. Blaabjerg, "Distributed primary and secondary power sharing in a droop-controlled LVDC microgrid with merged ac and dc characteristics," *IEEE Trans. Smart Grid*, vol. 9, no. 3, pp. 2284–2294, May 2018.

[23] H. Wang, M. Han, R. Han, J. M. Guerrero, and J. C. Vasquez, "A Decentralized current-sharing controller endows fast transient response to parallel DC–DC converters," *IEEE Trans. Power Electron.*, vol. 33, no. 5, pp. 4362–4372, May 2018.

[24] Z. Shuai, C. Shen, X. Liu, Z. Li, and Z. J. Shen, "Transient angle stability of virtual synchronous generators using Lyapunov's direct method," *IEEE Trans. Smart Grid*, vol. 10, no. 4, pp. 4648–4661, Jul. 2019.

[25] S. Sanchez and M. Molinas, "Large signal stability analysis at the common coupling point of a DC microgrid: A grid impedance estimation approach based on a recursive method," *IEEE Trans. Energy Convers.*, vol. 30, no. 1, pp. 122–131, Mar. 2015.

[26] X. Lu, K. Sun, J. M. Guerrero, J. C. Vasquez, L. Huang, and J. Wang, "Stability enhancement based on virtual impedance for dc microgrids with constant power loads," *IEEE Trans. Smart Grid*, vol. 6, no. 6, pp. 2770–2783, Nov. 2015.

[27] C. Yang, J. Sun, Q. Zhang, and X. Ma, "Lyapunov stability and strong passivity analysis for nonlinear descriptor systems," *IEEE Trans. Circuits Syst. I, Reg. Papers*, vol. 60, no. 4, pp. 1003–1012, Apr. 2013.

[28] H. Kim, S. Kang, G. Seo, P. Jang, and B. Cho, "Large-signal stability analysis of dc power system with shunt active damper," *IEEE Trans. Ind. Electron.*, vol. 63, no. 10, pp. 6270–6280, Oct. 2016.

[29] B. P. Loop, S. D. Sudhoff, S. H. Żak, and E. L. Zivi, "Estimating regions of asymptotic stability of power electronics systems using genetic algorithms," *IEEE Trans. Control Syst. Technol.*, vol. 18, no. 5, pp. 1011–1022, Sep. 2010.

[30] A. Bacha, H. Jerbi, and N. B. Braiek, "An approach of asymptotic stability domain estimation of discrete polynomial systems," in *Proc. Multiconf. Comput. Eng. Syst. Appl.*, 2006, vol. 1, pp. 288–292.

[31] R. K. Brayton and J. K. Moser, "A theory of nonlinear networks," *Quart. Appl. Math.*, vol. 22, pp. 1–33, 1964.

[32] K. Sun, L. Zhang, Y. Xing, and J. M. Guerrero, ''A distributed control strategy based on DC bus signaling for modular photovoltaic generation systems with battery energy storage," *IEEE Trans. Power Electron.*, vol. 26, no. 10, pp. 3032–3045, Oct. 2011.

[33] D. Wu, F. Tang, T. Dragičević, J. M. Guerrero, and J. C. Vasquez, ''Coordinated control based on bus-signaling and virtual inertia for islanded DC microgrids," *IEEE Trans. Smart Grid*, vol. 6, no. 6, pp. 2627–2638, Nov. 2015.

Wenqiang Xie (Student Member, IEEE) was born in Jiangsu, China, in 1993. He received the B.S. degree in 2016 from North China Electric Power University, Beijing, China, where he is currently working toward the Ph.D. degree in electrical engineering.

He is currently a Guest Ph.D. Student in the Department of Energy Technology, Aalborg University, Aalborg, Denmark. His research interests include power electronics, control, and their applications in dc microgrids.

Minxiao Han (Senior Member, IEEE) was born in Shannxi, China, in 1963. He received the Ph.D. degree from North China Electric Power University (NCEPU), Beijing, China, in 1995.

He was a Visiting Ph.D. Student with Queen's University of Belfast, U.K., and a Postdoctoral Fellow with Kobe University, Japan. He is currently the Director of Institute of Flexible Electric Power Technology, NCEPU. He has been the Leader in projects consigned by the National Nature Science Foundation of China, National Educational Ministry, and enterprises. He has published four books and more than 100 refereed publications in journals and conferences. His research interests include applications of power electronics in power system including HVDC, FACTS, power conversion and control.

Wenyuan Cao (Student Member, IEEE) was born in Hunan, China, in 1994. He received the B.S. degree in 2017 in North China Electric Power University, Beijing, China, where he is currently working toward the Ph.D. degree.

His research interests include hybrid ac/dc distribution network and its control.

Josep M. Guerrero (Fellow, IEEE) received the B.S. degree in telecommunications engineering, the M.S. degree in electronics engineering, and the Ph.D. degree in power electronics from the Technical University of Catalonia, Barcelona, Spain, in 1997, 2000 and 2003, respectively.

Since 2011, he has been a Full Professor with the Department of Energy Technology, Aalborg University, Aalborg, Denmark, where he is responsible for the Microgrid Research Program. Since 2014, he has been the Chair Professor with Shandong University, Jinan, China. Since 2015, he has been a Distinguished Guest Professor with Hunan University, Changsha, China. Since 2016, he has been a Visiting Professor Fellow with Aston University, Birmingham, U.K., and a Guest Professor with the Nanjing University of Posts and Telecommunications, Nanjing, China. Since 2019, he has been a Villum Investigator with The Villum Fonden, which supports the Center for Research on Microgrids (CROM) at Aalborg University, where he is the Founder and Director. He has authored and coauthored more than 500 journal papers in the fields of microgrids and renewable energy systems, which are cited more than 50 000 times. His research interests include different microgrid aspects, including power electronics, distributed energy-storage systems, hierarchical and cooperative control, energy management systems, smart metering, and the internet of things for ac/dc microgrid clusters and islanded minigrids, with a special focus on microgrid technologies applied to offshore wind and maritime microgrids for electrical ships, vessels, ferries, and seaports.

Dr. Guerrero is an Associate Editor for a number of IEEE Transactions. He was the recipient of the Best Paper Award of the IEEE TRANSACTIONS ON ENERGY CONVERSION for the period 2014–2015, the Best Paper Prize of IEEE-PES in 2015, the Best Paper Award of the IEEE JOURNAL OF POWER ELECTRONICS in 2016. From 2014 to 2019, he was awarded by Clarivate Analytics (former Thomson Reuters) as Highly Cited Researcher. In 2015, he was promoted as a fellow at the IEEE for his contributions on distributed power systems and microgrids.

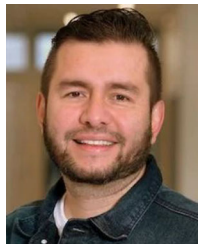

Juan C. Vasquez (Senior Member, IEEE) received the B.S. degree in electronics engineering from the Autonomous University of Manizales, Manizales, Colombia, in 2004, and the Ph.D. degree in automatic control, robotics, and computer vision from Barcelona Tech-UPC, Barcelona, Spain, in 2009.

In 2011, he was an Assistant Professor with the Department of Energy Technology, Aalborg University, Aalborg, Denmark, where he became an Associate Professor in 2014. In 2019, he became a Professor in Energy Internet and Microgrids and is currently the Co-Director of the Villum Center for Research on Microgrids. He was a Visiting Scholar with the Center of Power Electronics Systems (CPES), Virginia Tech, USA, and a Visiting Professor with Ritsumeikan University, Japan. His current research interests include operation, advanced hierarchical and cooperative control, optimization and energy management applied to distributed generation in ac/dc microgrids, maritime microgrids, advanced metering infrastructures and the integration of Internet of Things and Energy Internet into the smart grid. He has authored and coauthored more than 450 journal papers in the field of microgrids, which in total are cited more than 19 000 times.

Dr. Vasquez is an Associate Editor of *IET Power Electronics* and a Guest Editor of the IEEE TRANSACTIONS ON INDUSTRIAL INFORMATICS Special Issue on Energy Internet. He was awarded as Highly Cited Researcher by Thomson Reuters from 2017 to 2019 and was the recipient of the Young Investigator Award 2019. He is currently a member of the IEC System Evaluation Group SEG4 on LVDC Distribution and Safety for use in Developed and Developing Economies, the Renewable Energy Systems Technical Committee TC-RES in IEEE Industrial Electronics, PELS, IAS, and PES Societies.